



The wellbore is inclined from vertical, has a diameter typically  $\leq 0.3$  m and has length of the order  $\sim 10^3$  m. The cement is placed so as to completely fill the wellbore cross-section, either directly on top of drilling mud, already present in the hole, or alternatively above a specially designed *viscous pill* fluid. Cement and mud/viscous pill densities are *c.*  $1900 \text{ kg/m}^3$  and  $1200\text{--}1700 \text{ kg/m}^3$ , respectively. The situation described is mechanically unstable and without any mechanical support, two Newtonian fluids would exchange places. In order to keep the fluids in place, the rheologies are physio-chemically *designed* to be visco-plastic, (i.e., they exhibit a yield stress). One of the simplest rheological models with a yield stress is that of a Bingham fluid, which is assumed here. A similar modelling assumption has been taken in [2] and this is a common rheological model for oilfield flows of muds and cements.

Setting times for cements are many hours long. Excessive motion during setting will result in cement-mud contamination, which badly affects the integrity of the set cement plug. A clear question in designing the rheology of the viscous pill and/or cement slurry is, therefore, that of how large the yield stresses should be in order to maintain the fluids static. Completely general theoretical approaches to this question are difficult. The wellbore is a three-dimensional closed-ended pipe and the the interface topology can therefore be very complex. Experimental studies suggest that when the yield stresses are *close* to maintaining the fluids static, the type of flow which results is an elongated slumping motion, in which the heavy fluid moves down the lower side of the pipe, displacing the lighter fluid upwards, e.g., [3]. This observation justifies the use of two-fluid axial flow models, which prove much more amenable to analysis.

General features of axial duct flows of two Bingham fluids have been explored in a variational context in [4] and regularisation methods used to compute the axial velocity for various fixed interface configurations. In [5], the effects of yield stress variation were studied, with the focus specifically on the question of how large the yield stresses must be to achieve a static flow, (i.e., trivial solution). This approach was generalised to a wider class of axial flows, with significant normal deviatoric stresses, in [6], wherein favourable comparisons were also made with laboratory experiments. Whereas [4–6] consider pipe/duct geometries and fairly arbitrary interface configurations, a two-dimensional slot flow was analysed in [7]. With this simplified geometry, it is possible to derive analytic expressions, as a function of the two fluid yield stresses, for the heights of interface below and above which there can be no flow. For yield stresses larger than a certain curve, it was shown that for all interface heights, there are only trivial solutions. Close to these zero-flow bounds, perturbation solutions were derived, showing the necessity and sufficiency of these bounds.

In contrast to the above studies, the focus of this paper is on understanding transient motion in the slow axial slumping flows that have been described. This may at first appear irrelevant to the problem of plug-cementing stability, since clearly a static flow is desirable. However, when the yield stresses are not large enough for a static solution, it is perhaps still possible for the fluids to move so slowly that the cement can partially set, increasing the rheology and stabilising the flow. Allied to this possibility is the question of whether or not the unstable motion can be significantly influenced by variations in the plastic viscosities of the two fluids. This paper considers the transient versions of the problem in [7]. For simplicity, a slot geometry is chosen; a simplification which makes it possible to enter deeper into the problem and expose with clarity the mathematical structure of this type of two-fluid visco-plastic flow. Explained in particular is the significance of the set of zero solutions to the axial flow which was discovered in [7]. This mathematical structure appears to generalise to the fully three-dimensional transient two-fluid problem.

Bingham fluid flow problems have been considered widely in the recent mathematical and engineering literature. Aside from oilfield applications, visco-plastic fluid flows are fairly common in the chemical and food processing industries, as well as having agricultural and geological applications. A review of early work on Bingham fluid flows is given in [8], which also gives many of the known simple and classical flow solutions. There are also a growing number of process

engineering applications of axial flows of two fluids with differing rheologies, where one fluid essentially lubricates another and the fluids are pumped in ducts. A overview of these flows and a mathematical review of other relevant two-fluid flows can be found in [9,10].

The underlying mathematical theory for single Bingham fluid flows is developed in [11–13]. Spreading and interface motions of a single Bingham fluid on an inclined plane are considered in [14,15], which contain some interesting physical insights. Local analyses of some one-dimensional transient flows are presented in [16,17]. These papers are focused primarily on questions of stability and on the partial analogy between Bingham fluid flows and Stefan problems. Two recent papers [18,19] have considered different aspects of the displacement of Bingham fluids by inviscid fluids in a Hele-Shaw cell. The stability of stratified Bingham fluids in a Poiseuille flow have been considered in [20], which is a classical study of interface stability in a shear flow. Finally, local stability analysis of a *lubricated* Bingham-Newtonian axial flow is carried out in [21].

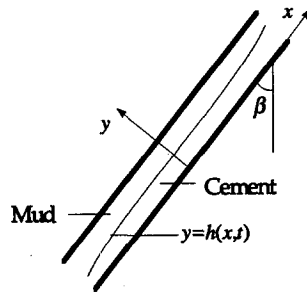


Figure 1. A schematic of the stratified exchange flows considered in this paper.

## 2. MODEL EQUATIONS

Consider a two-dimensional slot geometry and coordinates as shown in Figure 1. The slot axis is inclined at an angle  $\beta$  to the vertical direction of gravity and is assumed to contain a liquid cement slurry of density  $\hat{\rho}_c$  and a drilling mud of density  $\hat{\rho}_m$ . Its assumed that  $\hat{\rho}_c > \hat{\rho}_m$ . Suppose that the heavier fluid (cement) has initially been placed above ( $\hat{x}$  large and positive) the lighter fluid (mud). Under the action of gravity, the cement slides down the lower wall of the slot displacing the mud upwards against the upper wall of the slot. As this motion continues, the interface elongates into the situation shown in Figure 1. The fluids are assumed miscible, but not mixed. There are no interfacial forces, i.e., surface tension, and there is no mass transfer at the interface between mud and cement on the timescale of the motion. It is assumed that sufficiently far from the region of interest, the ends of the slot are closed. The fluids are incompressible and, consequently, there is no net axial flow of fluid across any slot cross-section. The flow of cement down the slot is balanced by an exchange flow of mud up the slot, see (3).

In [7], the following dimensionless equations are derived as a model for the above flow.

$$1 - f = \frac{\partial \tau_c}{\partial y}, \quad y \in [0, h), \quad (1)$$

$$-f = \frac{\partial \tau_m}{\partial y}, \quad y \in (h, 1], \quad (2)$$

$$Q \equiv \int_0^1 u \, dy = 0, \quad (3)$$

$$0 = \frac{\partial h}{\partial t} + \frac{\partial}{\partial x} Q_c(h). \quad (4)$$

The starting point for the model derivation is the Navier-Stokes equations. Coordinates  $(x, y)$  denote distance along the slot and perpendicularly across the slot, respectively. It is assumed that variations in the  $x$ -direction are much slower than those in  $y$ -direction, (i.e., the flow is

*long and thin*), and classical scaling arguments are then used to reduce the full set of equations. Equations (1) and (2) are the  $x$ -momentum equations in each fluid and equation (4) represents mass conservation, deriving from the kinematic condition and the incompressibility of the fluids.

The primitive solution variables are the modified pressure gradient  $f = f(x, t)$ , the  $x$ -component of velocity  $u = u(x, y, t)$ , (referred to later as the velocity), and the interface height  $h = h(x, t)$ . The function  $Q_c(h)$  in (4) is defined by

$$Q_c(h) \equiv \int_0^h u \, dy. \quad (5)$$

At each  $(x, t)$ , the interval  $[0, h]$  is assumed occupied by cement and the interval  $(h, 1]$  is assumed occupied by mud; see Figure 1. The shear stress in each fluid is denoted by  $\tau_k$ ,  $k = c, m$ . The rheologies of the two fluids are assumed to be governed by the Bingham model. Constitutive laws for each fluid are

$$\left| \frac{\partial u}{\partial y} \right| = 0 \iff |\tau_k| \leq \tau_{k,Y}, \quad (6)$$

$$\left| \frac{\partial u}{\partial y} \right| > 0 \implies \tau_k = \left[ \mu_k + \frac{\tau_{k,Y}}{\left| \frac{\partial u}{\partial y} \right|} \right] \frac{\partial u}{\partial y}, \quad (7)$$

where  $\tau_{k,Y}$ ,  $k = c, m$  denote the dimensionless yield stresses in each fluid and  $\mu_k$ ,  $k = c, m$  denote the dimensionless plastic viscosities of each fluid. The yield stresses are assumed positive and the plastic viscosities are assumed strictly positive, satisfying

$$\mu_c \mu_m = 1 \quad (8)$$

(which is due to selection of an appropriate velocity for scaling the dimensional equations).

Considering (7) and (8), it is seen that (1) and (2) are essentially second-order ordinary differential equations in  $y$ . No-slip boundary conditions are prescribed for  $u(x, y, t)$  at both walls:

$$u(x, 0, t) = u(x, 1, t) = 0. \quad (9)$$

Two further conditions are required. These come from continuity of shear stress and velocity at the interface, i.e.,

$$u(x, h, t) = u_{\text{int}}(x, t), \quad (10)$$

$$\tau_c(x, h, t) = \tau_m(x, h, t) = \tau_i(x, t), \quad (11)$$

by which it is understood that the interfacial velocity  $u_{\text{int}}(x, t)$  and interfacial shear stress  $\tau_i(x, t)$  are part of the solution, not the problem data. Evolution with time  $t$  enters only into (4). An initial condition for  $h(x, t)$  needs to be specified:

$$h(x, t) = h_0(x), \quad (12)$$

and it is assumed that  $h_0(x)$  is continuous and increasing, with  $h_0(-\infty) = 0$  and  $h_0(\infty) = 1$ , i.e.,  $h_0(x)$  separates regions of cement and mud as in Figure 1.

An interesting extension to the above system of equations is the fully transient axial flow problem, for which (1) and (2) are replaced by the following two partial differential equations:

$$e_c \frac{\partial u}{\partial t} + 1 - f = \frac{\partial \tau_c}{\partial y}, \quad y \in [0, h), \quad (13)$$

$$e_m \frac{\partial u}{\partial t} - f = \frac{\partial \tau_m}{\partial y}, \quad y \in (h, 1]. \quad (14)$$

An initial condition is required for  $u$ :

$$u(x, y, t) = u_0(x, y). \quad (15)$$

There are four different physically relevant problems which can be defined from the above system of equations.

- [U] (uncoupled and unconstrained). Equations (1) and (2) are solved, with (6) and (7) and using conditions (9)–(11). The interface position  $h$  and the modified pressure gradient  $f$  are considered as problem parameters. Other parameters are  $\tau_{k,Y}$ ,  $k = c, m$  and  $\mu_k$ ,  $k = c, m$ . The solution is the velocity  $u$ .
- [D] (decoupled and constrained). Equations (1) and (2) are solved, with (6) and (7) and using conditions (9)–(11). The interface position  $h$  is considered as a problem parameter. Other parameters are  $\tau_{k,Y}$ ,  $k = c, m$  and  $\mu_k$ ,  $k = c, m$ . The modified pressure gradient is determined by satisfying the constraint (3). The solution is the pair  $(u, f)$ .
- [C] (transient interface, coupled and constrained). Equations (1), (2), and (4) are solved, with (6) and (7) and using conditions (9)–(12). The problem parameters are  $\tau_{k,Y}$ ,  $k = c, m$  and  $\mu_k$ ,  $k = c, m$ . The modified pressure gradient is determined by satisfying the constraint (3). The solution is the triple  $(u, f, h)$ .
- [T] (fully transient, coupled and constrained). Equations (4), (13), and (14) are solved, with (6) and (7) and using conditions (9)–(12). The problem parameters are  $\tau_{k,Y}$ ,  $k = c, m$  and  $\mu_k$ ,  $k = c, m$ . The modified pressure gradient is determined by satisfying the constraint (3). The solution is the triple  $(u, f, h)$ . An initial condition for  $u$  is also required.

Each of the above problems contain free and/or moving boundaries. There are two different types of boundary here. First, there are the positions of possible yield surfaces in each fluid, i.e., where  $\tau_k = \pm\tau_{k,Y}$ . Second, there is the fluid-fluid interface position. Note that to solve [C], it is first necessary (or at least advisable) to solve [D]; problem [T] is less clear. This paper considers the transient interface and fluid motions associated with [C], and later also [T].

Previous work has essentially focused on a qualitative analysis of solutions to [U] and [D], fixing the interface position. In [7], the main focus is on defining sufficient conditions on the yield stresses  $(\tau_{c,Y}, \tau_{m,Y})$  to ensure that  $u = 0$  for [D]. It was shown that for values of  $(\tau_{c,Y}, \tau_{m,Y})$  which lie above the curve defined by

$$1 + (\tau_{c,Y} - \tau_{m,Y})^2 - 2(\tau_{c,Y} + \tau_{m,Y} + 2 \min\{\tau_{c,Y}, \tau_{m,Y}\}) = 0, \quad (16)$$

there can exist only the trivial solution  $u = 0$ . The curve (16) is plotted in Figure 2. For values of  $(\tau_{c,Y}, \tau_{m,Y})$  below (16) a nontrivial solution is only possible for certain values of  $h$ . These values are defined by

$$F(h, \tau_{c,Y}, \tau_{m,Y}) \equiv h(1-h) - (1-h)\tau_{c,Y} - h\tau_{m,Y} - \min\{\tau_{c,Y}, \tau_{m,Y}\} > 0, \quad (17)$$

i.e.,  $u \neq 0$  is possible for  $h \in (h_c, h_m)$ :

$$h_c = \frac{1 + \tau_{c,Y} - \tau_{m,Y} - \left[ (1 + \tau_{c,Y} - \tau_{m,Y})^2 - 4(\tau_{c,Y} + \min\{\tau_{c,Y}, \tau_{m,Y}\}) \right]^{1/2}}{2}, \quad (18)$$

$$h_m = \frac{1 + \tau_{c,Y} - \tau_{m,Y} + \left[ (1 + \tau_{c,Y} - \tau_{m,Y})^2 - 4(\tau_{c,Y} + \min\{\tau_{c,Y}, \tau_{m,Y}\}) \right]^{1/2}}{2}. \quad (19)$$

The variation of  $(h_c, h_m)$  with  $(\tau_{c,Y}, \tau_{m,Y})$  below (16) is shown in Figure 3. The solutions that are studied in this paper occupy the parameter envelope  $(h, \tau_{c,Y}, \tau_{m,Y})$  that is bounded by the two surfaces in Figure 3.

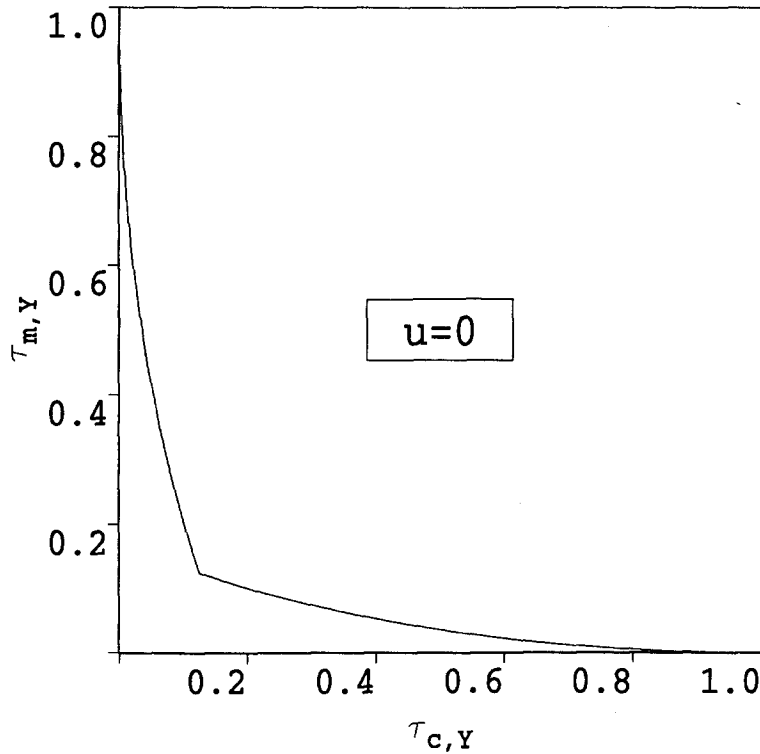


Figure 2. The curve in the  $(\tau_{c,Y}, \tau_{m,Y})$  plane defining where only  $u = 0$  is possible.

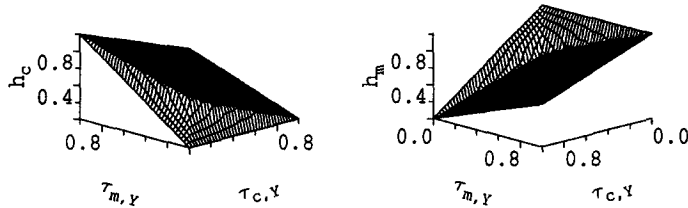


Figure 3. Variation in  $h_c$  and  $h_m$  with  $(\tau_{c,Y}, \tau_{m,Y})$ ; above (16)  $h^*$  is plotted.

Problems [U] and [D] are also members of a wider class of axial two-(Bingham) fluid duct flow problems. These are studied in a general context in [4,5]. Existence and uniqueness results for weak solutions are given in [4]. The solution  $u$  is shown to depend continuously on  $f$  and  $Q$  is shown to increase with  $f$ , implying that (3) can typically be used to determine  $f$ , and therefore, that [D] is sensible. The value of  $f$  which satisfies (3) is shown to also minimise the viscous dissipation functional  $a(u, u)$ :

$$a(u, u) = \mu_c \int_0^h \left( \frac{du}{dy} \right)^2 dy + \mu_m \int_h^1 \left( \frac{du}{dy} \right)^2 dy, \quad (20)$$

over all solutions  $u$  of [U]. In [5],  $u$  was shown to depend continuously on the yield stresses in various norms. Additionally,  $a(u, u)$  and other functionals representing plastic dissipation were shown to decrease with increasing  $\tau_{k,Y}$ ,  $k = c, m$ . This general behaviour is intuitive, in agreement with the more specific results in [7] and is qualitatively similar to that found for the axial flow of a single Bingham fluid, see e.g., [11–13]. Essentially, the implication is that for more or less arbitrary duct geometries, there exists a curve similar to (16), above which only trivial solutions exist.

Nontrivial solutions of [U] and [D] were computed in [4], for different interfaces fixed in pipe and eccentric annular geometries. However, in these geometries, solving the interface propagation problem [C] becomes overly difficult. The main focus of [5] was on finding trivial solutions to [D]

in an arbitrary duct. In [7], close to the curve (16) and/or for values of  $h$  close to the two surfaces in Figure 3, nontrivial perturbation solutions to [D] can be derived. Once away from these limits, analytic solution of [D]. (or even [U]) does not appear possible. Close to (16), the perturbation solutions can be used to define the function  $Q_c(h)$ , and consequently, [C] can also be analysed in the limit  $(h_m - h_c) \rightarrow 0$ :

$$Q_c(h) = \begin{cases} -\frac{1}{2\mu_c} \left[ \frac{1/4(h_m - h_c)^2 - (h - h^*)^2}{1 - h^* + h^*/\kappa + (1 - h^*)^{-0.5}} \right]^2, & \tau_{c,Y} < \tau_{m,Y}, \\ -\frac{1}{2\mu_c} \left[ \frac{1/4(h_m - h_c)^2 - (h - h^*)^2}{1 - h^* + h^*/\kappa + (h^*)^{-0.5}/\kappa} \right]^2, & \tau_{c,Y} > \tau_{m,Y}, \end{cases} \quad (21)$$

where

$$h_m + h_c \equiv 2h^*. \quad (22)$$

Note that  $Q_c(h) \equiv 0$ ,  $h \notin [h_c, h_m]$ . The function  $Q_c(h)$  in (21) has the shape of an inverted bell shape, vanishing smoothly to zero at both  $h_c$  and  $h_m$ . Using (21) in the interface propagation equation (4) gives solutions  $h(x, t)$  which become discontinuous from smooth initial conditions  $h_0(x)$ . In general, at sufficiently long times two *shocks* (i.e., discontinuities) will form and propagate in positive and negative directions along the slot. The heights  $h(x, t) = h^\pm$  and propagation speeds, say  $v^\pm$ , of the two discontinuities can be found analytically from the Rankine-Hugoniot conditions (see e.g., [22]), and are given by

$$h^\pm = h^* \pm \frac{1}{6} [h_m - h_c], \quad (23)$$

$$v^\pm = \pm \begin{cases} \frac{1}{27\mu_c} \left[ \frac{(h_m - h_c)^2}{1 - h^* + h^*/\kappa + (1 - h^*)^{-0.5}} \right]^2, & \tau_{c,Y} < \tau_{m,Y}, \\ \frac{1}{27\mu_c} \left[ \frac{(h_m - h_c)^2}{1 - h^* + h^*/\kappa + (h^*)^{-0.5}/\kappa} \right]^2, & \tau_{c,Y} > \tau_{m,Y}, \end{cases} \quad (24)$$

## 2.1. Dimensional Quantities

To aid with a physical interpretation of the results presented later, dimensional quantities can be recovered as follows. All lengths in the  $y$ -direction have been scaled with the slot width  $\hat{D}$ . Scaled yield stresses and plastic viscosities are defined by

$$\tau_{k,Y} = \frac{\hat{\tau}_{k,Y}}{\Delta\hat{\rho}\hat{g}\cos\beta\hat{D}}, \quad \mu_k = \frac{\hat{\mu}_k\hat{u}_*}{\hat{D}^2\Delta\hat{\rho}\hat{g}\cos\beta}, \quad k = c, m. \quad (25)$$

The dimensional quantities are denoted with a *hat* symbol;  $\Delta\hat{\rho}$  is the density difference between the fluids,  $\hat{g}$  is the gravitational acceleration,  $\beta$  is the slot inclination from vertical, and  $\hat{u}_*$  is the axial velocity scale. The latter is defined by

$$\hat{u}_* = \frac{\hat{D}^2\Delta\hat{\rho}\hat{g}\cos\beta}{[\hat{\mu}_c\hat{\mu}_m]^{1/2}}, \quad (26)$$

see (8). To recover the dimensional axial pressure gradient from  $f$ :

$$-f\Delta\hat{\rho}\hat{g}\cos\beta = \frac{d\hat{p}}{d\hat{x}} + \hat{\rho}_m\hat{g}\cos\beta. \quad (27)$$

Lengths in the axial  $x$ -direction have been scaled with an (arbitrary) length  $\hat{L} \gg \hat{D}$ . The timescale is then simply  $\hat{L}/\hat{u}_*$ . In equations (13) and (14), the constants  $e_k$  are defined by

$$e_k \equiv \frac{\hat{\rho}_k\hat{u}_*^2}{\Delta\hat{\rho}\hat{g}\cos\beta\hat{L}}, \quad k = c, m. \quad (28)$$

### 3. COMPUTING THE FLUX FUNCTION $Q_C$

The natural method of solving [C] is to first compute  $Q_c(h)$  at each  $h$ , via solution of problem [D], and then to integrate (4). The computation of  $Q_c(h)$  and its subsequent approximation must therefore be sufficiently accurate to act as data for (4). The perturbation solution (21) suggests that shock discontinuities will occur when solving (4). For equations such as (4), it is known that these weak solutions very often characterise the general solution behaviour at long times. Consequently, computation of the function  $Q_c(h)$  should be accurate enough to be able to find the positions and speeds of the shock discontinuities.

#### 3.1. A Minimisation Formulation for Problem [D]

For fixed  $h$ , integrating (1) and (2) produces

$$\tau_c(y) = y(1-h) + (1-y)\tau_{c,w} + y\tau_{m,w}, \quad y \in [0, h), \quad (29)$$

$$\tau_m(y) = h(1-y) + (1-y)\tau_{c,w} + y\tau_{m,w}, \quad y \in (h, 1], \quad (30)$$

where  $\tau_{c,w}$  and  $\tau_{m,w}$  are the values of  $\tau_c(y)$  and  $\tau_m(y)$  at  $y = 0$  and  $y = 1$ , respectively, i.e., the shear stresses at the walls. In integrating (1) and (2),  $f$  has been eliminated by

$$f = h + \tau_{c,w} - \tau_{m,w}, \quad (31)$$

and the interfacial stress condition (11) is satisfied with

$$\tau_i = h(1-h) + (1-h)\tau_{c,w} + h\tau_{m,w}. \quad (32)$$

Equations (6) and (7) with equations (29) and (30) define the velocity gradient pointwise for  $y \in [0, h)$  and  $y \in (h, 1]$ . These expressions for the velocity gradient may be integrated using the no-slip boundary conditions (9), at  $y = 0$  for the interval  $y \in [0, h)$ , and at  $y = 1$  for the interval  $y \in (h, 1]$ . This integration gives a velocity field in each interval and, in particular,  $u_{\text{int},c}(h, \tau_{c,w}, \tau_{m,w})$  and  $u_{\text{int},m}(h, \tau_{c,w}, \tau_{m,w})$ , which are the limiting values of  $u$  at  $h$ , from either side of the interface. Further integration of the two velocity field in each interval gives  $Q_c(h, \tau_{c,w}, \tau_{m,w})$  and  $Q_m(h, \tau_{c,w}, \tau_{m,w})$ , the latter being defined by

$$Q_m \equiv \int_h^1 u(x, y, t) dy = Q - Q_c. \quad (33)$$

Note that the solutions found depend on  $(\tau_{c,w}, \tau_{m,w})$ . Note also that there is no guarantee that either (3) or (10) will be satisfied. To accomplish this, the function  $Z(h, \tau_{c,w}, \tau_{m,w})$ , defined by

$$Z(h, \tau_{c,w}, \tau_{m,w}) = \|\mathbf{z}_c - \mathbf{z}_m\|^2, \quad (34)$$

$$\mathbf{z}_c(h, \tau_{c,w}, \tau_{m,w}) = \begin{bmatrix} u_{\text{int},c}(h, \tau_{c,w}, \tau_{m,w}) \\ -Q_c(h, \tau_{c,w}, \tau_{m,w}) \end{bmatrix}, \quad (35)$$

$$\mathbf{z}_m(h, \tau_{c,w}, \tau_{m,w}) = \begin{bmatrix} u_{\text{int},m}(h, \tau_{c,w}, \tau_{m,w}) \\ Q_m(h, \tau_{c,w}, \tau_{m,w}) \end{bmatrix} \quad (36)$$

is minimised, with  $Z(h, \tau_{c,w}, \tau_{m,w}) = 0$  being necessary and sufficient for (3) and (10).

#### 3.2. Computation and Minimisation of $Z(h, \tau_{c,w}, \tau_{m,w})$

A number of different errors can contribute to computation of the functional  $Z(h, \tau_{c,w}, \tau_{m,w})$  and its subsequent minimisation. A fully analytical solution is not possible. However, errors in computing  $u_{\text{int},c}(h, \tau_{c,w}, \tau_{m,w})$ ,  $u_{\text{int},m}(h, \tau_{c,w}, \tau_{m,w})$ ,  $Q_c(h, \tau_{c,w}, \tau_{m,w})$ , and  $Q_m(h, \tau_{c,w}, \tau_{m,w})$ , can be minimised using the following pseudo-algorithm.

1. From (29) and (30), find exactly the positions  $y$  where  $\tau_c(y) = \pm\tau_{c,Y}$  and  $\tau_m(y) = \pm\tau_{m,Y}$ .

2. Divide the interval  $[0, h]$  into subintervals on each of which either  $\tau_c(y) > \tau_{c,Y}$  or  $\tau_c(y) < -\tau_{c,Y}$  or  $|\tau_c(y)| \leq \tau_{c,Y}$ . Divide the interval  $(h, 1]$  into subintervals on each of which either  $\tau_m(y) > \tau_{m,Y}$  or  $\tau_m(y) < -\tau_{m,Y}$  or  $|\tau_m(y)| \leq \tau_{m,Y}$ . Use (6) and (7) to define the velocity gradient.
3. Integrate on each subinterval numerically using a second-order quadrature or better, to find the velocity at the endpoints of each subinterval. Do this sequentially beginning at the walls and ending at the interface, giving  $u_{\text{int},c}(h, \tau_{c,w}, \tau_{m,w})$  and  $u_{\text{int},m}(h, \tau_{c,w}, \tau_{m,w})$ .
4. Transform the integrals for  $Q_c$  and  $Q_m$  by integrating by parts:

$$\int_{y_1}^{y_2} u \, dy = [yu] \Big|_{y_1}^{y_2} - \int_{y_1}^{y_2} y \frac{du}{dy} \, dy.$$

Evaluate each integral numerically using a 3<sup>rd</sup> order quadrature or better.

The velocity profile for a Bingham fluid flow of the type considered is continuous in each fluid and is piecewise quadratic, joined at the yield surfaces. The above procedure minimises possible errors at the ends of each subinterval, due to discontinuities in the higher derivatives. Using the orders of quadrature indicated, the integrations are exact. Thus,  $Z(h, \tau_{c,w}, \tau_{m,w})$  is evaluated exactly (i.e., with machine precision) using for example, Simpson's rule.

The minimisation problem is solved using a standard algorithm for the unconstrained minimisation of a sum of squares, taken from the NAG Fortran library, subroutine E04FDF. This is found to work reasonably well, with residual

$$Z(h, \tau_{c,w}^*, \tau_{m,w}^*) \approx 10^{-23},$$

for the solution  $(\tau_{c,w}, \tau_{m,w}) = (\tau_{c,w}^*, \tau_{m,w}^*)$ , over a broad range of  $(h, \tau_{c,w}, \tau_{m,w})$ . If problems are found with the minimisation, it is typically if either  $h_m - h_c \ll 1$ , (i.e., close to the curve in Figure 2, or if  $h \sim h_c$  or  $h \sim h_m$ . In these two limits, the set of feasible  $(\tau_{c,w}, \tau_{m,w})$  vanishes, as does the velocity  $u$ .

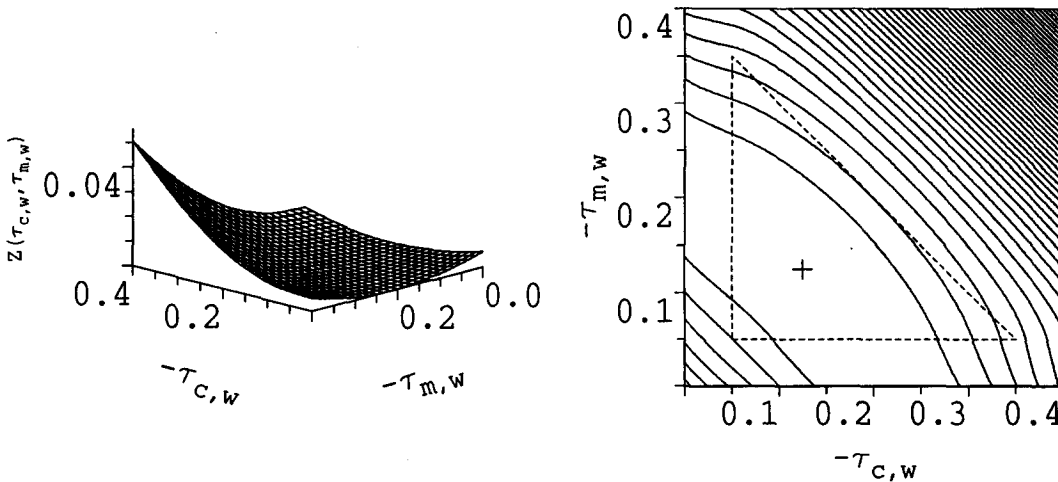


Figure 4. The function  $Z(h, \tau_{c,w}, \tau_{m,w})$  for  $\tau_{k,Y} = 0.05$ ,  $\mu_k = 1$ ,  $h = 0.5$ ; (a) surface plot, (b) contour plot with spacings at  $\Delta Z = 0.001$ , the triangular region sketched illustrates a physical constraint set for the solution, (marked +).

Figure 4 shows an objective function  $Z(h, \tau_{c,w}, \tau_{m,w})$  for parameters:  $\tau_{k,Y} = 0.05$ ,  $\mu_k = 1$ ,  $h = 0.5$ . This type of function is typical of a case for which the optimisation works well. A typical function  $Z(h, \tau_{c,w}, \tau_{m,w})$  when the minimisation is *difficult* is shown in Figure 5. Parameters for Figure 5 are  $\tau_{k,Y} = 0.05$ ,  $\mu_k = 1$ ,  $h = 0.12$ , and here  $(h_c, h_m) \approx (0.1127, 0.8873)$ . Some

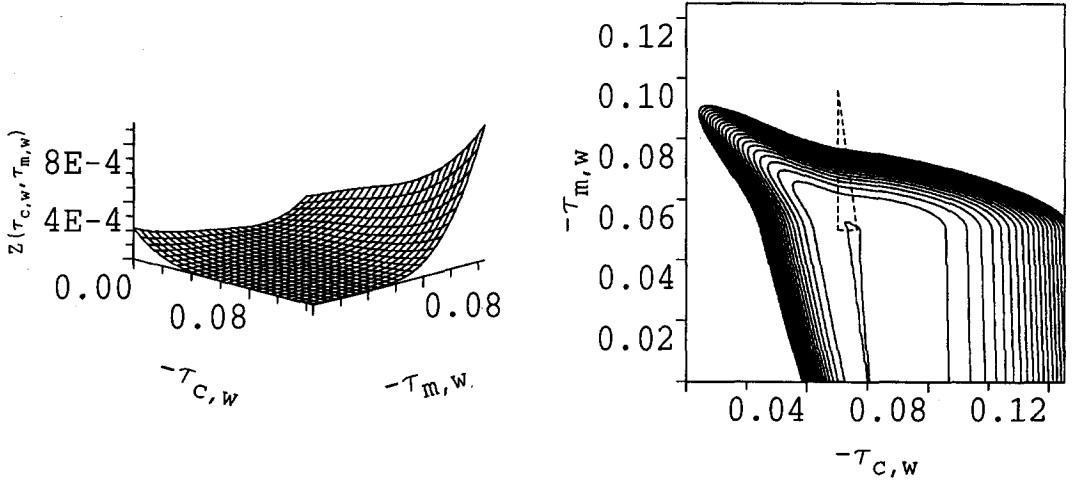


Figure 5. The function  $Z(h, \tau_{c,w}, \tau_{m,w})$  for  $\tau_{k,Y} = 0.05$ ,  $\mu_k = 1$ ,  $h = 0.12$ , with here  $h_c \approx 0.1127$ ; (a) surface plot, (b) contour plot with spacings at  $\Delta Z = 10^{-9} + j * 10^{-7}$ ,  $j = 0, \dots, 20$ , the triangular region sketched illustrates a physical constraint set for the solution.

comparison can be made with Figure 4, since only  $h$  has changed. Note that the axes scales are smaller in Figure 5. The first contour drawn in Figure 5 is  $Z(h, \tau_{c,w}, \tau_{m,w}) = 10^{-9}$  and the second is  $Z(h, \tau_{c,w}, \tau_{m,w}) = 10^{-7}$ . The intersection of the first contour with the triangular feasibility region pinpoints the solution. Clearly, the objective function becomes very flat in these vanishing limits and the precise evaluation of  $Z(h, \tau_{c,w}, \tau_{m,w})$  becomes critical for the performance of the minimisation.

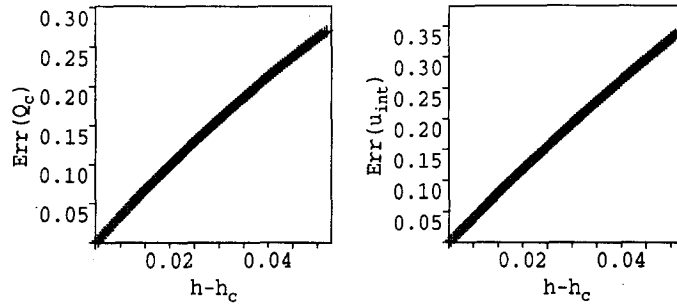


Figure 6. Comparison of the solution to the minimisation problem with a perturbation solution for  $h \sim h_c$ :  $\mu_k = 1$ ,  $(\tau_{c,Y}, \tau_{m,Y}) = (0.02, 0.4)$ ; (a) relative error in  $Q_c(h)$ , (b) relative error in  $u_{\text{int}}(h)$ .

To construct a solution that is valid over the full range of feasible  $(h, \tau_{c,Y}, \tau_{m,Y})$ , the numerical solution can be combined with the perturbation solutions in [7]. Figure 6 shows the normalised error between the numerical solution to the optimisation  $(Q_c(h), u_{\text{int}})$  and the perturbation solution  $(Q_{c,\text{pert}}(h), u_{\text{int,pert}})$ . The region  $h \sim h_c$  is considered for  $\mu_k = 1$ ,  $(\tau_{c,Y}, \tau_{m,Y}) = (0.02, 0.4)$ . Here  $(h_c, h_m) \approx (0.0731, 0.5469)$  and  $(Q_c(h), u_{\text{int}}(h))$  have been evaluated at 1000 points in the interval  $(h_c, h_m)$ . The functions  $\text{Err}(Q_c)$  and  $\text{Err}(u_{\text{int}})$  which have been plotted are defined by

$$\text{Err}(Q_c) = \left| 1 - \frac{Q_c}{Q_{c,\text{pert}}} \right|, \quad \text{Err}(u_{\text{int}}) = \left| 1 - \frac{u_{\text{int}}}{u_{\text{int,pert}}} \right|, \quad (37)$$

and note that  $Q_{c,\text{pert}} \sim |h - h_k|^2$  and  $u_{\text{int,pert}} \sim |h - h_k|^2$  as  $|h - h_k| \rightarrow 0$ ;  $k = c, m$ . Figure 6 shows that the numerical and analytical solutions can be patched together in this way and is also a good test of accuracy for the numerical solution. For the parameters chosen in Figure 6, the

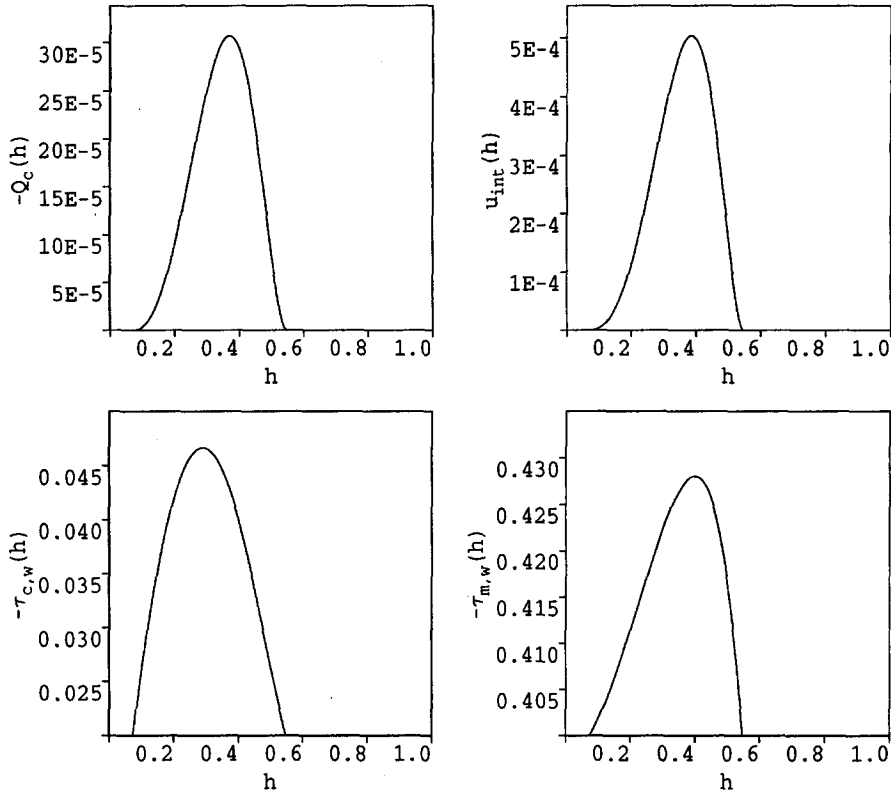


Figure 7. Solution to the minimisation problem for  $\mu_k = 1$ ,  $(\tau_{c,Y}, \tau_{m,Y}) = (0.02, 0.4)$ ; (a)  $Q_c(h)$ , (b)  $u_{int}(h)$ , (c)  $\tau_{c,w}^*(h)$ , (d)  $\tau_{m,w}^*(h)$ .

minimisation has worked very well, even close to the endpoints of  $(h_c, h_m)$ . When this is not the case, significant numerical error typically remains confined to the last few points computed.

Figure 7 shows typical functions  $Q_c(h)$ ,  $u_{int}(h)$ ,  $\tau_{c,w}(h)$ , and  $\tau_{m,w}(h)$  that are computed by the above procedure, for the same parameters as in Figure 6. Although the four curves are qualitatively similar, note that those for  $Q_c(h)$  and  $u_{int}(h)$  are defined fully for  $h \in [0, 1]$ , whereas those for  $\tau_{c,w}(h)$  and  $\tau_{m,w}(h)$  are only defined for  $h \in (h_c, h_m) \approx (0.0731, 0.5469)$ . At each end of this interval,  $\tau_{c,w}(h) \rightarrow -\tau_{c,Y}$  and  $\tau_{m,w}(h) \rightarrow -\tau_{m,Y}$ , the fluids no longer yield and the stresses become indeterminate. After the solution to the minimisation problem has been found, the velocity profile can be computed straightforwardly from (1) and (2) at each  $h$ . These are second-order differential equations which may be integrated using the boundary conditions  $u = 0$  at the wall, the interface velocity  $u_{int}(h)$  and with  $f(h)$  defined in terms of the solution  $\tau_{c,w}^*(h)$  and  $\tau_{m,w}^*(h)$  by (31). It has been shown in [7] that the velocity profile always has one of the three characteristic profiles illustrated in Figure 8; computing the exact profile adds little insight.

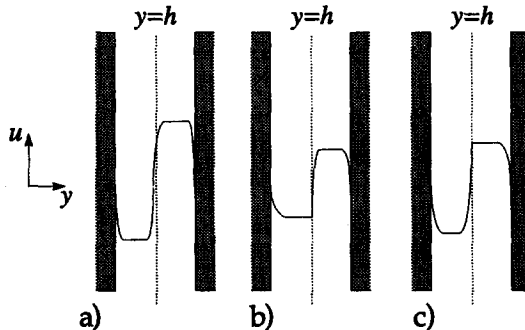


Figure 8. Schematic of the different possible velocity profiles.

### 3.3. Characterisation of $Q_c(h)$

For  $(\tau_{c,Y}, \tau_{m,Y})$  lying below the curve (16), it is found that  $Q_c(h)$  can be characterised generally as follows.

1.  $Q_c(h) \leq 0$ , with  $Q_c(h) < 0$  only for  $h \in (h_c, h_m)$ .
2. At the ends of the interval  $(h_c, h_m)$ , the convergence of  $Q_c(h)$  to zero is quadratic, i.e.,  $Q_c(h) \sim -A_c(h - h_c)^2$  and  $Q_c(h) \sim -A_m(h - h_m)^2$  for constants  $A_c, A_m$ , (which are defined by the perturbation solutions in [7]).
3.  $Q_c(h) \in C_0^1[0, h]$ , but  $Q_c(h) \notin C_0^2[0, h]$ , due to discontinuities in the second derivatives at  $h_c$  and  $h_m$ .
4.  $Q_c(h)$  has a single minimum, at say  $h = h_{Q\min}$  and two points of inflexion, say  $h_{i,c}$  and  $h_{i,m}$ , with  $h_{i,c} \in (h_c, h_{Q\min})$  and  $h_{i,m} \in (h_{Q\min}, h_m)$ .

Under these conditions, it is clear that the characteristics of a classical solution will eventually intersect, after which time only a weak solution will exist. There is the possibility of a shock discontinuity forming in each of the intervals  $(h_c, h_{Q\min})$  and  $(h_{Q\min}, h_m)$ . Denoting the heights and speeds of the shocks again by  $h^\pm$  and  $v^\pm$ , these quantities are found from the characteristic equation and the Rankine-Hugonit conditions, which for this problem give

$$(1 - h^+) v^+ = -Q_c(h^+), \quad (38)$$

$$h^- v^- = Q_c(h^-), \quad (39)$$

$$v^+ = \frac{dQ_c}{dh}(h^+), \quad (40)$$

$$v^- = \frac{dQ_c}{dh}(h^-). \quad (41)$$

For  $Q_c(h)$  as characterised, it is not hard to show that there exist unique  $h^+$  and  $h^-$ . For example, note that  $h^-$  is a zero of the function

$$h \frac{dQ_c}{dh}(h) - Q_c(h). \quad (42)$$

This function is continuous, is strictly positive for  $h \in [h_{Q\min}, h_m)$  and strictly negative as  $h \rightarrow h_c$ . Also, the derivative of the function (42) is given by

$$\frac{d^2 Q_c}{dh^2}(h),$$

which is strictly negative for  $h \in (h_c, h_{i,c})$  and strictly positive for  $h \in (h_{i,c}, h_{Q\min})$ . Consequently, (42) is strictly negative at  $h_{i,c}$  and must have a single zero for  $h \in (h_{i,c}, h_{Q\min})$ , which defines  $h^-$ . A similar analysis shows that there is a single  $h^+ \in (h_{Q\min}, h_{i,m})$ .

## 4. INTERFACE MOTION; PROBLEM [C]

Equation (4) is a nonlinear hyperbolic conservation equation. Numerical methods for the solution of such equations are many, e.g., see [22] for an up-to-date account. The method used here is taken from the recent work of Cockburn and Shu [23]. The algorithms discussed in [23] each couple a compact (i.e., implicit) spatial differencing scheme with a Runge-Kutta type of time discretisation. The method implemented here uses third-order upwinded compact differencing and third-order Runge-Kutta time differencing, i.e., the overall scheme is third order in both time and space. The modification to the minimod function that is discussed in [23] is exactly that which is implemented here. In [23], various results are proven regarding the (total variation) stability of this scheme. In implementing this scheme, the test problem results in [23] were first reproduced, before the method was applied to equation (4). The authors have found that this

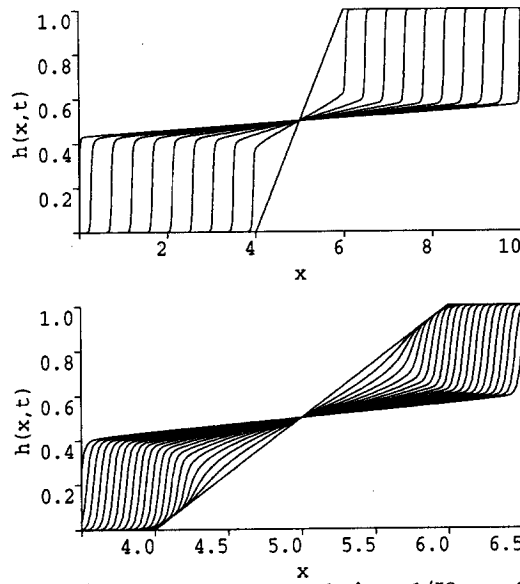


Figure 9. Profiles of  $h(x, t)$  for  $\tau_{k, \gamma} = 0.05$ ,  $\mu_k = 1$ ,  $\Delta x = 1/50$ ,  $\alpha \approx 9.407 \times 10^{-3}$ ; (a)  $h(x, t)$  plotted every 100 timesteps, (b) initial interface evolution,  $h(x, t)$  plotted every ten timesteps.

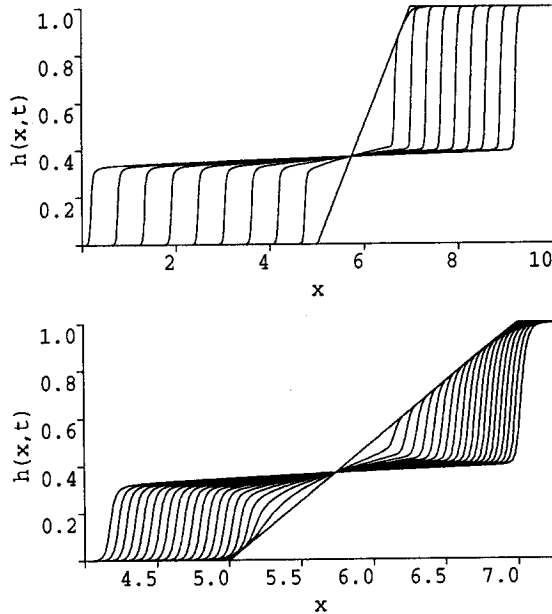


Figure 10. Profiles of  $h(x, t)$  for  $(\tau_{c, \gamma}, \tau_{m, \gamma}) = (0.02, 0.4)$ ,  $\mu_k = 1$ ,  $\Delta x = 1/50$ ,  $\alpha \approx 2.769 \times 10^{-3}$ ; (a)  $h(x, t)$  plotted every 200 timesteps, (b) initial interface evolution,  $h(x, t)$  plotted every 20 timesteps.

scheme performs consistently well in computing the solution to (4). This is a fairly comprehensive test, since (4) contains two shocks which form and move in opposite directions and since the flux function  $Q_c(h)$  is numerically computed. The only slightly unsatisfactory feature of the scheme was in computing an amount of numerical smoothing close to the shocks at both  $h = 0$  and  $h = 1$ , (see Figures 9–11). This effect appears consistent, (i.e., diminishes with mesh refinement), did not affect interface propagation behaviour and the smoothed regions did not grow at all with time. Possibly the smoothing is a consequence of the compact spatial differencing scheme, which involves a form of spatial averaging. This was not investigated in detail, but seems likely to be the case since changing the order of Runge-Kutta time differencing had little effect on the phenomena.

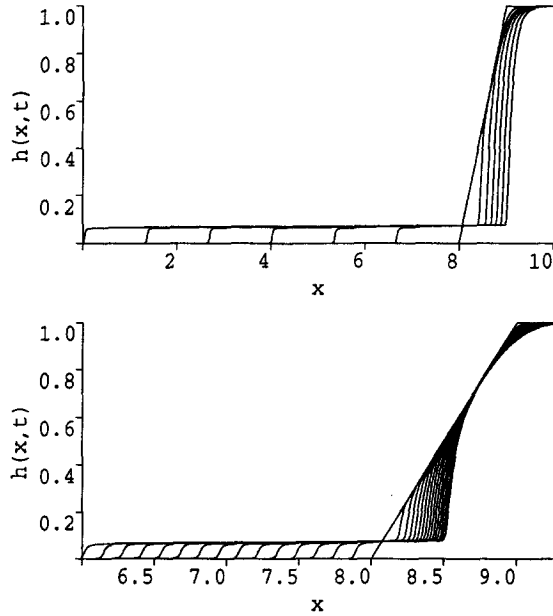


Figure 11. Profiles of  $h(x, t)$  for  $(\tau_{c,Y}, \tau_{m,Y}) = (0, 0.9)$ ,  $\mu_k = 1$ ,  $\Delta x = 1/100$ ,  $\alpha \approx 4.02 \times 10^{-5}$ ; (a)  $h(x, t)$  plotted every 1000 timesteps, (b) initial interface evolution,  $h(x, t)$  plotted every 100 timesteps.

Three examples serves to illustrate the characteristic behaviour of solutions to problem [C]. For all results presented,  $\mu_k = 1$ . In the first example, equal yield stresses are taken. A slot of length 10 is considered and initial conditions are at the slot centre:

$$h_0(x) = \begin{cases} 0, & x \leq 4, \\ 0.5(x - 4), & 4 < x < 6, \\ 1, & x \geq 6. \end{cases} \quad (43)$$

The mesh spacing chosen is  $\Delta x = 1/50$  and the following CFL condition is satisfied:

$$\Delta t = K_{\text{CFL}} \frac{\Delta x}{\alpha} \quad (44)$$

with  $K_{\text{CFL}} = 0.45$ , ( $K_{\text{CFL}} = 0.5$  is sufficient for stability), where

$$\alpha = \sup_{h \in [0,1]} \left| \frac{dQ_c}{dh}(h) \right|. \quad (45)$$

Figure 9 shows the results of this computation. The interface is tracked over 1000 timesteps; Figure 9a plots the interface after every 100 timesteps, Figure 9b plots the interface at every ten timesteps for  $x \in [3.5, 6.5]$ , showing the initial interface evolution into the shock profile. The shocks propagate left and right at identical speeds and distances from the walls of the slot, as would be expected from the choice of identical rheological parameters.

For the second example,  $(\tau_{c,Y}, \tau_{m,Y}) = (0.02, 0.4)$ , the interval  $(h_c, h_m) \approx (0.0731, 0.5469)$  and the flux function  $Q_c(h)$  is that shown in Figure 7. Initial conditions are

$$h_0(x) = \begin{cases} 0, & x \leq 5, \\ 0.5(x - 5), & 5 < x < 7, \\ 1, & x \geq 7. \end{cases} \quad (46)$$

In Figure 10, the interface propagation is no longer symmetric. Since (3) is still satisfied, the smaller shock propagates faster than the larger shock. It is interesting to note that although

the interface propagates significantly slower than in Figure 9, the discontinuities appear after the interface has moved a similar length along the slot, i.e., more or less directly after the effect of the initial conditions has been left behind. For the the final example,  $(\tau_{c,Y}, \tau_{m,Y}) = (0, 0.9)$ , for which  $(h_c, h_m) = (0, 0.1)$ . Initial conditions were

$$h_0(x) = \begin{cases} 0, & x \leq 8, \\ x - 8, & 8 < x < 9, \\ 1, & x \geq 9. \end{cases} \quad (47)$$

Figure 11 shows the computed solution, for which a thin layer of cement forces its way along the lower wall of the slot, displacing the mud very slowly upwards, (i.e., increasing  $x$ ).

It is quite impractical to study parametric variation of solutions to [C] with direct computations of the interface motion, i.e., as in Figures 9–11. In these computations, it has been found that convergence of the solutions to the weak solutions is relatively rapid, in terms of the distance travelled from the initial profile. Thus, all the essential information regarding the movement of the interface at long times, (meaning long axial distances), is given by the weak solutions. Interface motion at long times can therefore be described as follows.

If the point  $(\tau_{c,Y}, \tau_{m,Y})$  lies below the curve (16), then there will be shock discontinuities at  $h^-(\tau_{c,Y}, \tau_{m,Y}, \kappa)$  and  $h^+(\tau_{c,Y}, \tau_{m,Y}, \kappa)$ , which propagate down and up the slot at speeds  $v^-(\tau_{c,Y}, \tau_{m,Y}, \kappa)$  and  $v^+(\tau_{c,Y}, \tau_{m,Y}, \kappa)$ , respectively. Here  $\kappa$  is the viscosity ratio:

$$\kappa \equiv \frac{\mu_c}{\mu_m}, \quad (48)$$

which is the only other problem parameter, (recall that (8) is also satisfied by  $\mu_c$  and  $\mu_m$ ). Integrating  $v^-$  and  $v^+$  with respect to time, the position of these discontinuities can be followed, say at  $x^-(\tau_{c,Y}, \tau_{m,Y}, \mu_c/\mu_m, t)$  and  $x^+(\tau_{c,Y}, \tau_{m,Y}, \mu_c/\mu_m, t)$ . At sufficiently large times,  $h = 0$  for  $x < x^-(t)$  and  $h = 1$  for  $x > x^+(t)$ . The interface for  $x \in [x^-(t), x^+(t)]$  is simply stretched between the two values  $h^-$  and  $h^+$ .

It is worth remarking that this motion is slightly contrary to the simplistic notion of motion that results from direct consideration of solutions to [D], where nonzero  $Q_c$  and  $u$  are found only in the interval  $(h_c, h_m)$ . Intuitively, only values of  $h$  in this interval will move. The weak solutions allow the whole interface to propagate. In fact, the interval  $(h_c, h_m)$  determines only a bound for the interval  $(h^-, h^+)$ , in which the interface is stretched. For  $\kappa = 1$ , Figure 12 shows the variation in  $v^\pm(\tau_{c,Y}, \tau_{m,Y}, \kappa)$  and in  $h_m - h^+(\tau_{c,Y}, \tau_{m,Y}, \kappa)$  and  $h^-(\tau_{c,Y}, \tau_{m,Y}, \kappa) - h_c(\tau_{c,Y}, \tau_{m,Y})$ . It is noticeable that the interval  $(h^-, h^+)$  is typically much smaller than  $(h_c, h_m)$ , so that the stretching motion is confined to a thin  $h$ -layer between the propagating shocks.

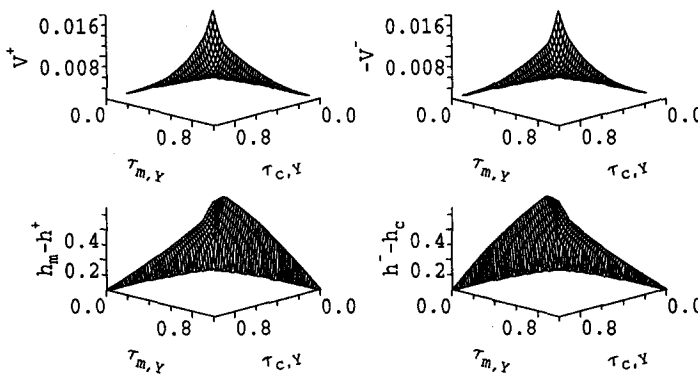


Figure 12. Variation in shock speeds  $v^+(\tau_{c,Y}, \tau_{m,Y}, \kappa)$ ,  $v^-(\tau_{c,Y}, \tau_{m,Y}, \kappa)$ , and in shock heights  $h_m - h^+(\tau_{c,Y}, \tau_{m,Y}, \kappa)$  and  $h^-(\tau_{c,Y}, \tau_{m,Y}, \kappa) - h_c$  for  $\kappa = 1$ .

Also noticeable in Figure 12 is that the shock speed increases rapidly with distance from the curve (16). Perhaps not surprisingly, the maximum value of the shock speeds is when the fluids are both Newtonian. Taking as typical parameters:  $\hat{D} \approx 0.1$ ,  $\Delta\hat{\rho} \approx 300 \text{ kg/m}^3$ , and  $\hat{\mu}_c \approx \hat{\mu}_m \approx 50 \text{ cPo}$ , with a near vertical slot, the velocity scale is  $\hat{u}_* \approx 500 \text{ m/s}$ . Consequently, this peak propagation velocity will be of the order of  $8 \text{ m/s}$ . The implication is that, for typical parameters, if the yield stresses are not sufficiently high to lie above the curve (16), the flow will propagate *fast*. Of course, sufficiently close to (16), it is possible to have arbitrarily *slow* propagation, but in terms of a yield stress variation below (16), it is clearly necessary that the yield stresses are very close to (16) to have any propagation speed that might usefully allow the cement slurry to partially set (say a speed less than  $0.01 \text{ m/s}$  might be thought of *slow*). On the other hand, the velocities for this type of axial flow are much lower than might be expected. The velocity scale is based on the balance between viscous and gravitational effects and a naive view would expect the propagation speeds to be  $\sim 1$ .

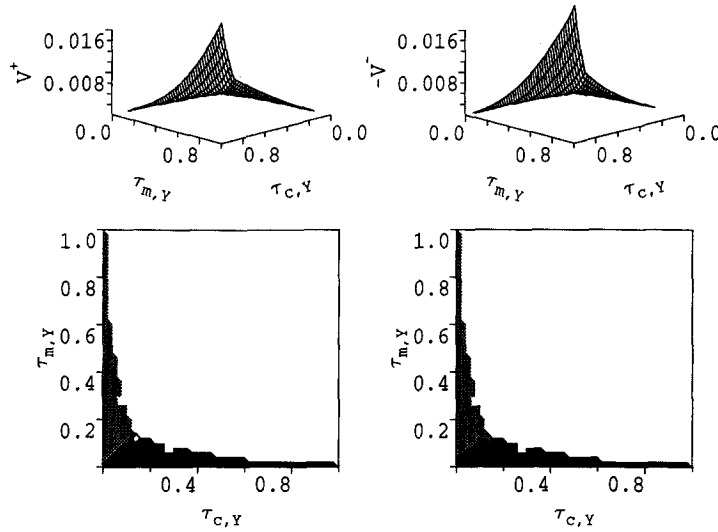


Figure 13.  $\kappa = 1/10$ : (a)  $v^+(\tau_{c,Y}, \tau_{m,Y}, \kappa)$ , (b)  $v^-(\tau_{c,Y}, \tau_{m,Y}, \kappa)$ , (c)  $v^+(\tau_{c,Y}, \tau_{m,Y}, \kappa)/v^+(\tau_{c,Y}, \tau_{m,Y}, 1)$ , (d)  $v^-(\tau_{c,Y}, \tau_{m,Y}, \kappa)/v^-(\tau_{c,Y}, \tau_{m,Y}, 1)$ :  $v^\pm(\tau_{c,Y}, \tau_{m,Y}, \kappa)/v^\pm(\tau_{c,Y}, \tau_{m,Y}, 1) > 1$  is shaded light and  $v^\pm(\tau_{c,Y}, \tau_{m,Y}, \kappa)/v^\pm(\tau_{c,Y}, \tau_{m,Y}, 1) < 1$  is shaded dark.

Figures 13 and 14 show the effects of changing the viscosity ratio on the shock propagation speeds  $\kappa = 1/10$  and  $\kappa = 10$ , (i.e., in Figure 13, the mud plastic viscosity is ten times that of the cement). It is clear that there is a form of asymmetry about the line  $\tau_{c,Y} = \tau_{m,Y}$  and between  $v^\pm(\tau_{c,Y}, \tau_{m,Y}, \kappa)$  in Figure 12 between Figures 13 and 14. This type of asymmetry is also evident in (21).

Over the range  $\kappa$  considered, the differences in propagation speeds are not enormous. In the lower parts of Figures 13 and 14, there are shown contour plots of the ratios  $v^+(\tau_{c,Y}, \tau_{m,Y}, \kappa)/v^+(\tau_{c,Y}, \tau_{m,Y}, 1)$  and  $v^-(\tau_{c,Y}, \tau_{m,Y}, \kappa)/v^-(\tau_{c,Y}, \tau_{m,Y}, 1)$ . All that is shown in these plots is those regions of the  $(\tau_{c,Y}, \tau_{m,Y})$ -plane where  $v^+(\tau_{c,Y}, \tau_{m,Y}, \kappa)/v^+(\tau_{c,Y}, \tau_{m,Y}, 1) > 1$  (shaded light) and where  $v^+(\tau_{c,Y}, \tau_{m,Y}, \kappa)/v^+(\tau_{c,Y}, \tau_{m,Y}, 1) < 1$  (shaded dark). Close to (16) calculating these ratios suffers from numerical problems, i.e., since  $v^\pm(\tau_{c,Y}, \tau_{m,Y}, \kappa) \rightarrow 0$ . From these lower plots, one can draw what general conclusions are possible about viscosity effects. Roughly speaking, when not close to the line  $\tau_{c,Y} = \tau_{m,Y}$ .

- For  $\mu_c < \mu_m$ , propagation speeds are slower if  $\tau_{c,Y} < \tau_{m,Y}$  and faster if  $\tau_{c,Y} > \tau_{m,Y}$ .
- For  $\mu_c > \mu_m$ , propagation speeds are slower if  $\tau_{c,Y} > \tau_{m,Y}$  and faster if  $\tau_{c,Y} < \tau_{m,Y}$ , (i.e., faster/slower in comparison to the case  $\mu_c = \mu_m$ ).

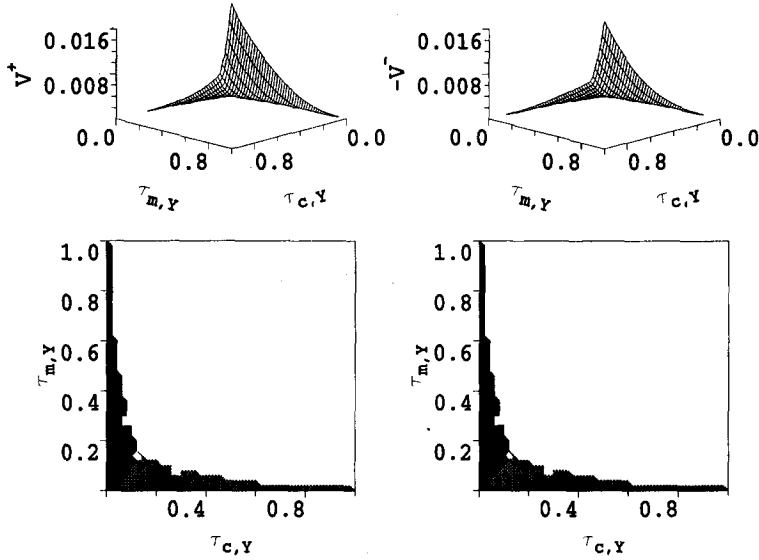


Figure 14.  $\kappa=10$ : (a)  $v^+(\tau_{c,Y}, \tau_{m,Y}, \kappa)$ , (b)  $v^-(\tau_{c,Y}, \tau_{m,Y}, \kappa)$ , (c)  $v^+(\tau_{c,Y}, \tau_{m,Y}, \kappa)/v^+(\tau_{c,Y}, \tau_{m,Y}, 1)$ , (d)  $v^-(\tau_{c,Y}, \tau_{m,Y}, \kappa)/v^-(\tau_{c,Y}, \tau_{m,Y}, 1)$ :  $v^\pm(\tau_{c,Y}, \tau_{m,Y}, \kappa)/v^\pm(\tau_{c,Y}, \tau_{m,Y}, 1) > 1$  is shaded light and  $v^\pm(\tau_{c,Y}, \tau_{m,Y}, \kappa)/v^\pm(\tau_{c,Y}, \tau_{m,Y}, 1) < 1$  is shaded dark.

Perhaps this is because, for example, taking  $\mu_c < \mu_m$  and  $\tau_{c,Y} < \tau_{m,Y}$  has the unambiguous effect of *viscosifying* the cement layer and condition (3) guarantees that the mud layer flow also slows down. In contrast,  $\mu_c < \mu_m$  and  $\tau_{c,Y} > \tau_{m,Y}$  might allow some form of lubrication.

More general statements about the effects of plastic viscosity variations do not seem possible to make. The difficulty is because plastic viscosity effects are hard to uncouple from yield stress effects, but not vice-versa. For an axial flow of a Bingham fluid, the yield stress determines the positions and thickness of the yield surfaces; in the unyielded region of the flow, the viscosity plays no role whatsoever, this role is confined to the sheared fluid layers. Perhaps an analysis based on this type of underlying analysis would define the effects of viscosity more clearly. However, it is also likely to be inaccessible to intuitive insight and in this case one must question its utility.

## 5. THE FULLY TRANSIENT PROBLEM [T]

Analysis of problem [T] will be kept purely formal and is only qualitative, although a numerical solution to [T] is not thought to present any particular problems. The analysis is carried out within a variational framework, which is simpler and adequate for the current purposes. It is believed that the type of local stability analysis in [16,17,21] could also be adapted to this problem. In considering [T], note that at each axial position  $x$ , the velocity  $u$  satisfies the following variational inequality:

$$e(u_t, v - u) + a(u, v - u) + j(v) - j(u) \geq -Q_c(v - u), \quad \forall v \in V, \quad u \in S, \quad (49)$$

where  $a(u, v - u)$  is defined by (20) and

$$e(w, v - u) = e_c \int_0^h w(v - u) dy + e_m \int_h^1 w(v - u) dy, \quad (50)$$

$$j(v) = \tau_{c,Y} \int_0^h \left| \frac{du}{dy} \right| dy + \tau_{m,Y} \int_h^1 \left| \frac{du}{dy} \right| dy. \quad (51)$$

Test space and solution spaces are

$$v(y) \in V = \{w \in H_0^1[0, 1] : Q(w) = 0\}, \quad (52)$$

$$u(y, t) \in S = \{w \in V : w \in L^2[0, T], w_t \in L^2[0, T]\}. \quad (53)$$

Note here that  $V = V(h)$  and  $S = S(h)$ , since the operators  $a$ ,  $e$ , and  $j$  rely on the interface height for their definitions. Meanwhile, the velocity solution to the *steady* problem [D], say  $u_s$ , satisfies the variational inequality

$$a(u_s, v - u_s) + j(v) - j(u_s) \geq -Q_c(v - u_s), \quad \forall v \in V, \quad u_s \in V. \quad (54)$$

For a derivation of these inequalities, see [4,11].

The first simple result is to note that the difference between the two solutions,  $\Delta u$ ,

$$\Delta u \equiv u_s - u \quad (55)$$

satisfies

$$e([\Delta u]_t, \Delta u) + a(\Delta u, \Delta u) \leq 0. \quad (56)$$

A bound for  $a(\Delta u, \Delta u)$  is given by the Poincaré inequality

$$a(\Delta u, \Delta u) \geq \min\{\mu_k\} \pi^2 \|\Delta u\|_{L^2_{[0,1]}}^2, \quad (57)$$

and using the mean value theorem

$$e([\Delta u]_t, \Delta u) = \frac{\bar{e}(t)}{2} \frac{\partial}{\partial t} \|\Delta u\|_{L^2_{[0,1]}}^2, \quad (58)$$

for some  $\bar{e}(t) \in (\min\{e_k\}, \max\{e_k\})$ . Thus,

$$\frac{\partial}{\partial t} \|\Delta u\|_{L^2_{[0,1]}}^2 \leq -\frac{2 \min\{\mu_k\} \pi^2}{\max\{e_k\}} \|\Delta u\|_{L^2_{[0,1]}}^2 \quad (59)$$

and on integrating with respect to  $t$ :

$$\|\Delta u\|_{L^2_{[0,1]}}^2(t) \leq \|\Delta u\|_{L^2_{[0,1]}}^2(0) e^{-2\lambda_\mu t}, \quad (60)$$

where

$$\lambda_\mu = \frac{\min\{\mu_k\} \pi^2}{\max\{e_k\}}. \quad (61)$$

Consequently, as  $t \rightarrow \infty$ ,  $\|\Delta u\|_{L^2_{[0,1]}}(t) \rightarrow 0$  exponentially, at a rate controlled by the plastic viscosities of the fluids. This means that if the solution of the steady problem [D] is  $u_s = 0$ , e.g., if the yield stresses lie above the curve (16), then the transient solution also converges to zero. Apart from at the two shock positions, there appears to be no problem to extend this result to the solutions of problem [C]. At each  $h \neq h^\pm$ , the velocity solution also satisfies (54) and the convergence of  $u$  to the solutions of [C] therefore follows. Eventually one would expect the interface in [T] to propagate in the same way as in [C]. However, at short times, there is clearly the possibility of interaction between this convergence behaviour and shock propagation, resulting in complicated solution behaviours. This is possibly a good reason not to attempt a full numerical solution. Probably, the most useful parameter range for this type of analysis is for  $(\tau_{c,Y}, \tau_{m,Y})$  above the curve (16), where solutions to both [D] and [C] are trivial and the convergence of [T] is nonambiguous.

Supposing that  $(\tau_{c,Y}, \tau_{m,Y})$  lie above the curve (16), it is possible to obtain a faster convergence result for  $u$  to zero. In this region, the yield stresses help in a direct way to damp the transients. Note that  $u$  satisfies the equality

$$e(u_t, u) + a(u, u) + j(u) = -Q_c(u), \quad (62)$$

and consequently,

$$\frac{\bar{e}(t)}{2} \frac{\partial}{\partial t} \|u\|_{L^2_{[0,1]}}^2 + \min\{\mu_k\} \pi^2 \|u\|_{L^2_{[0,1]}}^2 \leq -Q_c(u) - j(u). \quad (63)$$

Supposing that  $Q_c(u) \neq 0$ , then

$$-Q_c(u) - j(u) \leq \frac{1}{2} \|u\|_{L^1_{[0,1]}} \left[ 1 - 2 \frac{j(u)}{\|u\|_{L^1_{[0,1]}}} \right] \leq \frac{1}{2} \|u\|_{L^1_{[0,1]}} \left[ 1 - 2 \inf_{v \in V, v \neq 0} \left\{ \frac{j(v)}{\|v\|_{L^1_{[0,1]}}} \right\} \right]. \quad (64)$$

For  $v \in V, v \neq 0$ , the ratio  $j(v)/\|v\|_{L^1_{[0,1]}}$  can always be scaled, so that the space  $v \in V, |Q_c(v)| = 1$  can be considered equivalently. This ratio should be minimised by functions that are constant on as large as possible a part of the interval  $[0, 1]$ , minimising the contribution to  $j(v)$ . However, continuity conditions must be satisfied at the interface and the boundary conditions must also be satisfied. Restricting any variation from a piecewise constant function, to thin strips, of width  $\epsilon$ , close to the interface and boundaries, it appears that the infimum of  $j(v)/\|v\|_{L^1_{[0,1]}}$  is attained by the limit as  $\epsilon \rightarrow 0$  of the sequence  $v_\epsilon$ :

$$v_\epsilon(y) = \begin{cases} -\frac{y}{h\epsilon} + O(\epsilon), & y \in [0, \epsilon], \\ -\frac{1}{h} + O(\epsilon), & y \in [\epsilon, h - \epsilon], \\ -\frac{1}{h} + O(\epsilon), & y \in (h - \epsilon, h], \text{ if } \tau_{c,Y} \geq \tau_{m,Y}, \\ -\frac{1}{h} + \frac{y - h + \epsilon}{\epsilon} \left[ \frac{1}{1 - h} + \frac{1}{h} \right] + O(\epsilon), & y \in (h - \epsilon, h], \text{ if } \tau_{c,Y} < \tau_{m,Y}, \\ \frac{1}{1 - h} + \frac{y - h - \epsilon}{\epsilon} \left[ \frac{1}{1 - h} + \frac{1}{h} \right] + O(\epsilon), & y \in [h, h + \epsilon), \text{ if } \tau_{m,Y} \leq \tau_{c,Y}, \\ \frac{1}{1 - h} + O(\epsilon), & y \in [h, h + \epsilon), \text{ if } \tau_{m,Y} > \tau_{c,Y}, \\ \frac{1}{1 - h} + O(\epsilon), & y \in [h + \epsilon, 1 - \epsilon], \\ \frac{1 - y}{\epsilon(1 - h)} + O(\epsilon), & y \in (1 - \epsilon, 1]. \end{cases} \quad (65)$$

The  $O(\epsilon)$  terms in the definition of  $v_\epsilon$  are chosen so that  $Q_c = -1, Q_m = 1$  and the slightly complex behaviour at the interface ensures that  $v_\epsilon$  changes sign in the fluid with the smaller yield stress, again minimising the contribution to  $j(v_\epsilon)$ . With this assumption:

$$\begin{aligned} -Q_c(u) - j(u) &\leq \frac{1}{2} \|u\|_{L^1_{[0,1]}} \left[ 1 - \frac{1}{h(1 - h)} \min\{\tau_{k,Y}\} - \frac{1}{h} \tau_{c,Y} - \frac{1}{1 - h} \tau_{m,Y} \right] \\ &= \frac{1}{2} \|u\|_{L^1_{[0,1]}} \frac{F(h, \tau_{c,Y}, \tau_{m,Y})}{h(1 - h)}, \end{aligned} \quad (66)$$

where  $F(h, \tau_{c,Y}, \tau_{m,Y})$  is as defined in (17). If  $F(h, \tau_{c,Y}, \tau_{m,Y}) < 0, \forall h \in [0, 1]$ , the convergence of  $u \rightarrow 0$  is clearly accelerated. This condition is exactly that which defines the zero-flow curve (16).

To get a precise convergence estimate, the above procedure can be used to derive the following inequality:

$$\begin{aligned} \frac{\bar{e}(t)}{2} \frac{\partial}{\partial t} \|u\|_{L^2_{[0,1]}}^2 + \min\{\mu_k\} \pi^2 \|u\|_{L^2_{[0,1]}}^2 &\leq -Q_c(u) - j(u) \\ &\leq \frac{1}{2} \|u\|_{L^2_{[0,1]}} \left[ 1 - 2 \inf_{v \in V, \|v\|_{L^1_{[0,1]}} = 2} \left\{ \frac{j(v)}{\|v\|_{L^2_{[0,1]}}} \right\} \right]. \end{aligned} \quad (67)$$

Assuming that the sequence  $v_\epsilon$  again converges to give this infimum, (not so clear):

$$\frac{\bar{e}(t)}{2} \frac{\partial}{\partial t} \|u\|_{L^2_{[0,1]}}^2 + \min\{\mu_k\} \pi^2 \|u\|_{L^2_{[0,1]}}^2 \leq \frac{1}{2} \|u\|_{L^2_{[0,1]}} \tilde{F}(h, \tau_{c,Y}, \tau_{m,Y}), \quad (68)$$

where

$$\tilde{F}(h, \tau_{c,Y}, \tau_{m,Y}) \equiv \left[ \frac{[h(1-h)]^{1/2} - 2[\min\{\tau_{k,Y}\} + (1-h)\tau_{c,Y} + h\tau_{m,Y}]}{[h(1-h)]^{1/2}} \right]. \quad (69)$$

Thus, if the yield stresses are such that

$$\tilde{F}(h, \tau_{c,Y}, \tau_{m,Y}) \leq -2\Delta\tau < 0, \quad \forall h \in [0, 1],$$

then it follows that

$$\bar{e}(t) \frac{\partial}{\partial t} \|u\|_{L^2_{[0,1]}}^2 + \min\{\mu_k\} \pi^2 \|u\|_{L^2_{[0,1]}}^2 \leq -\Delta\tau \quad (70)$$

and

$$\|u\|_{L^2_{[0,1]}}(t) \leq \left( \|u\|_{L^2_{[0,1]}}(0) + \frac{\lambda_\tau}{\lambda_\mu} \right) e^{-\lambda_\mu t} - \frac{\lambda_\tau}{\lambda_\mu}, \quad (71)$$

$$\|u\|_{L^2_{[0,1]}}(t) = 0, \quad \text{if } t \geq \frac{1}{\lambda_\mu} \left( 1 + \frac{\lambda_\mu \|u\|_{L^2_{[0,1]}}(0)}{\lambda_\tau} \right), \quad (72)$$

where

$$\lambda_\tau \equiv \frac{\Delta\tau}{\max\{e_k\}}. \quad (73)$$

Therefore, for sufficiently large  $\tau_{k,Y}$ , the flow will stop in a finite time, controlled essentially by the magnitude of the yield stresses  $\Delta\tau$ .

A concluding remark is to note that the above type of argument is a generalisation to two fluids of the stability results for a single fluid, see [11,13]. For a single fluid, there is a single value of the dimensionless yield stress which determines global asymptotic stability of the system. For two fluids, global asymptotic stability is given by the curve (16). The result also appears generalisable to three-dimensional flows of two fluids, (i.e., the real situation in a wellbore), which have an analogous variational formulation. Equation (62) becomes the three-dimensional energy equation and the operators are defined slightly differently. The argument then relies on the ellipticity of  $a(\cdot, \cdot)$  in three dimensions and on the evaluation of the appropriate infima. It is the latter which presents the real technical difficulty: in one dimension, it was necessary to maximise  $F(h, \tau_{c,Y}, \tau_{m,Y})$  over  $h$  to find (16). The three-dimensional equivalent must consider the variation of all possible interfaces, i.e., it is a type of minimal surface problem. Regardless of this difficulty, it appears that the global asymptotic stability of the fully three-dimensional transient two-fluid problem will be defined parametrically by finding the set of zero solutions to the analogous slow flow problem.

## REFERENCES

1. C. Marca, Remedial cementing, In *Well Cementing*, (Edited by E.B. Nelson), Chapter 13, Schlumberger Educational Services, Houston, TX, (1990).
2. R.M. Beirute, Flow behaviour of an unset cement plug in place, Society of Petroleum Engineers, Paper Number SPE 7589 (1978).
3. D.G. Calvert, J.F. Heathman and J.E. Griffith, Plug cementing: Horizontal to vertical conditions, Society of Petroleum Engineers, Paper Number SPE 30514 (1995).
4. I.A. Frigaard and O. Scherzer, Uniaxial exchange flows of two Bingham fluids in a cylindrical duct, *IMA J. Appl. Math.* **61**, 237–266 (1998).
5. I.A. Frigaard and O. Scherzer, The effects of yield stress variation on uniaxial exchange flows of two Bingham fluids in a pipe, *SIAM J. Appl. Math.* (to appear); Technical report 6/1998, Industrial Mathematics Institute, University of Linz, Austria (1998).

6. I.A. Frigaard and J.P. Crawshaw, Preventing buoyancy driven flows of two Bingham fluids in a closed pipe: Fluid rheology design for oilfield plug, *J. Engng. Math.* (to appear).
7. I.A. Frigaard, Stratified exchange flows of two Bingham fluids in an inclined slot, *J. Non-Newtonian Fluid Mech.* **78**, 61–87 (1998).
8. R. Byron-Bird, G.C. Dai and B.J. Yarusso, The rheology and flow of viscoplastic materials, *Reviews in Chemical Engineering* **1** (1), 1–70 (1983).
9. D.D. Joseph and Y.Y. Renardy, *Fundamentals of Two-Fluid Dynamics, Part 1: Mathematical Theory and Applications*, Springer-Verlag, (1991).
10. D.D. Joseph and Y.Y. Renardy, *Fundamentals of Two-Fluid Dynamics, Part 2: Lubricated Transport, Drops and Miscible Liquids*, Springer-Verlag, (1991).
11. G. Duvaut and J.L. Lions, *Inequalities in Mechanics and Physics*, Volume 219, pp. 279–327, Springer-Verlag, (1976).
12. R. Glowinski, J.L. Lions and R. Tremolieres, *Numerical Analysis of Variational Inequalities*, North-Holland, Amsterdam, (1981).
13. R. Glowinski, *Numerical Methods for Nonlinear Variational Problems*, Springer-Verlag, (1983).
14. K.F. Liu and C.C. Mei, Slow spreading of a sheet of Bingham fluid on an inclined plane, *J. Fluid Mech.* **207**, 505–529 (1989).
15. K.F. Liu and C.C. Mei, Roll waves on a layer of a muddy fluid flowing down a gentle slope—A Bingham model, *Phys. Fluids* **6**, 2577–2590 (1994).
16. E. Comparini, A one-dimensional Bingham flow, *J. Math. Anal. & Appl.* **169**, 127–139 (1992).
17. E. Comparini and E. de Angelis, Flow of a Bingham fluid in a concentric cylinder viscometer, *Advances in Mathematical Sciences and Applications* **6** (1), 97–116 (1996).
18. A.N. Alexandrou and V. Entov, On the steady state advancement of fingers and bubbles in a Hele-Shaw cell filled by a non-Newtonian fluid, *Euro. Jnl. of Applied Mathematics* **8**, 73–87 (1997).
19. V.A. Gorodtsov and V.M. Yentov, Instability of the displacement fronts of non-Newtonian fluids in a Hele-Shaw cell, *J. Appl. Maths. Mechs.* **61** (1), 111–126 (1997).
20. A. Pinarbasi and A. Liakopoulos, Stability of two-layer Poiseuille flow of Carreau-Yasuda and Bingham-like fluids, *J. Non-Newtonian Fluid Mech.* **57**, 227–241 (1995).
21. E. Comparini and P. Mannucci, Flow of a Bingham fluid in contact with a Newtonian fluid (Preprint) (1997).
22. D. Kröner, *Numerical Schemes for Conservation Laws*, Wiley-Teubner, (1997).
23. B. Cockburn and C.-W. Shu, Nonlinearly stable compact schemes for shock calculations, *SIAM J. Numer. Anal.* **31** (3), 607–627 (1994).